

Scalable Neural Tangent Kernel of Recurrent Architectures

Sina Alemohammad, Randall Balestriero, Zichao Wang, and Richard Baraniuk
Rice University, Houston, Texas, USA
{sa86, rb42, zw16, richb}@rice.edu

Abstract—Kernels derived from deep neural networks (DNNs) in the infinite-width provide not only high performance in a range of machine learning tasks but also new theoretical insights into DNN training dynamics and generalization. In this paper, we extend the family of kernels associated with recurrent neural networks (RNNs), which were previously derived only for simple RNNs, to more complex architectures that are bidirectional RNNs and RNNs with average pooling. We also develop a fast GPU implementation to exploit its full practical potential. While RNNs are typically only applied to time-series data, we demonstrate that classifiers using RNN-based kernels outperform a range of baseline methods on 90 non-time-series datasets from the UCI data repository.

Index Terms—Neural tangent kernel, Recurrent neural network, Gaussian process, Overparameterization, Kernel methods.

I. INTRODUCTION

Deep neural networks (DNNs) have proven to be unreasonably effective at solving a range of machine learning problems when one has access to a large collection of training data. While research has long focused on the empirical performance of DNN methods, theoretical research is increasingly focusing on the interpretability of these models using rigorous mathematical principles.

One major research thread has focused on the *infinite-width regime* of DNNs with Gaussian initialization, where DNNs are shown to be in correspondence with kernels machines. It is widely known that the output of a single-hidden-layer feed-forward neural network converges to a Gaussian Process (GP) with an associated Conjugate Kernel (CK) (also known as NN-GP kernel) as the number of units (neurons) in the hidden layer goes to infinity [1]. This result has been proven to hold for other DNN architectures as well [2]–[6].

While the CK models DNNs at initialization without any training, recent studies have also linked trained DNNs to kernels. In particular, it has been shown that infinite width DNNs with Gaussian initialization trained with gradient descent converges to a kernel ridge regression predictor with respect to a kernel known as the *neural tangent kernel* (NTK) [7], [8]. These results allow one to interpret DNNs with powerful tools from kernels, and has facilitated the analysis of DNNs generalization performances [9]–[12].

The kernel interpretation of DNNs allows to design algorithms using DNN-inspired kernels that are potentially more powerful than classical kernels and other algorithms such as random forest (RF) on datasets of small sizes (typically less than 5000 data points) [13]. Several other works has also investigated the practicality of kernels derived from DNNs on larger datasets where it has been shown that NTK and CK can outperform trained finite-width DNNs [4], [14]–[16].

While there are ample theoretical and empirical results on the DNNs with fully connected or convolutional structure, recurrent neural networks (RNNs) received only little attention in the realm of NTKs. RNNs are widely used architectures and constitute the foundation of many modern applications including language translation, speech transcription and audio processing [17]–[19]. NTK and CK of RNN have provided practitioners with a novel similarity measure able to handle input data sequences of different lengths; and as also been used successfully for kernel ridge regression [20]

and dimensionality reduction of time-series data [21]. This makes the need to enrich the family of kernels associated to RNNs even more crucial to extend the many insightful results already developed for non recurrent architectures.

Recently, [20], [22] derived the kernel associated to a simple RNN coined the *recurrent neural tangent kernel* (RNTK). Those studies only focused on the vanilla RNN, leaving out a number of other types of more powerful RNN variants such as bidirectional RNNs [23]. Those more complex architectures are crucial to study in the infinite width regime as they correspond to models leading to higher performances in the finite width regime. Allowing a direct performance comparison between different RNN models and in both infinite and finite width regime is important to grasp the impact of depth in those models. Furthermore, extending the family of CKs and NTKs is also crucial to effectively measure the performance gap between those two kernel families. In this study, we propose to enrich the family of RNTKs by deriving and analysis the kernels associated to more complex RNN architectures.

Contributions. In this paper, we extend the existing works on infinite width RNNs and summarize our contributions as follows:

[C1] Building upon previous works that derived the CK and NTK of multi-layer simple RNNs [20], we derive the CK and NTK of other RNN extensions including bi-directional RNN (BI-RNN), average pooling RNN (RNN-AVG) and their combination, BI-RNN-AVG.

[C2] We provide the code to calculate the CK and NTK of RNNs and its mentioned variants when all data have the same length. The code can be executed on CPU or GPU in a unified code by using the library SymJAX [24].

[C3] We show superior performance of infinite-width RNN-based kernels compared to other classical kernels and NTKs on a wide range of non time-series datasets. This result along with the provided GPU implementation should encourage the use of NTK and CK of RNNs (and its variants) in various applications.

[C4] In [2], it has been observed that kernel ridge regression with CK typically outperforms NTK on a variety of datasets. We empirically show that, CK and NTK of RNNs and its variants and MLP achieve a similar performance when SVM training is used, instead of kernel ridge regression.

II. BACKGROUND

We first introduce notations and review key concepts of NTK, RNNs and kernels (CK and NTK) associated to infinite width RNNs which will aid the development of the kernels of different RNN variants.

A. Kernels For Infinite-width DNNs

In this section we introduce two kernels that are associated to infinite-width DNNs, namely CK and NTK.

Given a DNN with a single output and with parameters (weights) θ denoted by $f_\theta(\mathbf{x})$ and a pair of inputs \mathbf{x} and \mathbf{x}' , the CK is defined as:

$$\mathcal{K}(\mathbf{x}, \mathbf{x}') := \mathbb{E}_{\theta \sim \mathcal{N}} [f_\theta(\mathbf{x}) \cdot f_\theta(\mathbf{x}')], \quad (1)$$

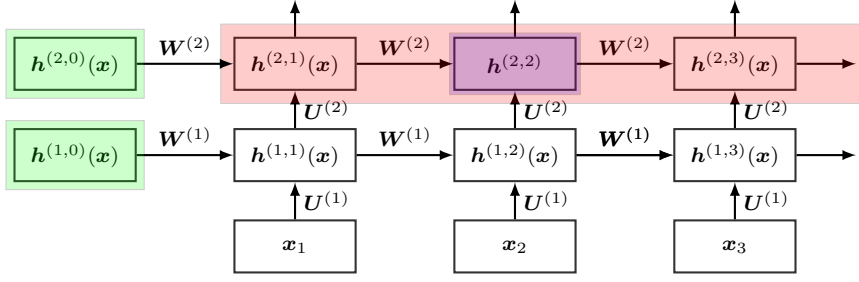


Fig. 1: Visualization of an RNN that highlights a cell (purple), a layer (red), and the initial hidden state of each layer (green). (Best viewed in color.)

where θ is Gaussian distributed. The GP prior induced on the output of DNN enables Bayesian inference in regression tasks [2], and is equivalent to a *weakly-trained* DNN e.g, when only the last layer (readout layer) is trained using gradient descent on the square loss [8].

Recent studies have focused on the *fully-trained* infinite-width DNNs, where all of the parameters are trained using gradient descent. In this setting, it has been shown that DNNs evolve as a linear model during training. More precisely, for parameters close to initialization, θ_0 , we can use a first-order Taylor expansion:

$$f_{\theta}^{\text{lin}}(\mathbf{x}) \approx f_{\theta_0}(\mathbf{x}) + \langle \nabla_{\theta} f_{\theta_0}(\mathbf{x}), \theta - \theta_0 \rangle,$$

and use this linearized model for training. In such setting, the dynamics of training using gradient descent is equivalent to kernel gradient descent on the function space with respect to the NTK formulated as

$$\Theta(\mathbf{x}, \mathbf{x}') := \langle \nabla_{\theta} f_{\theta}(\mathbf{x}), \nabla_{\theta} f_{\theta}(\mathbf{x}') \rangle. \quad (2)$$

for any DNN architecture [7], [8].

Each DNN architecture produces a distinct NTK due to the inherent structural biases of the different layers (convolutional, fully-connected, residual, recurrent). NTKs have been derived for multiple DNN architectures, including multilayer perceptrons (MLPs) [7], convolutional neural networks (CNNs) [15], [25], residual neural networks (ResNets) [26], graph neural networks (GNNs) [27], and more recently recurrent neural networks (RNNs) [20], [25], [28]. In [6], [28], the author provides a general methodology to derive both the CK and NTK for any DNN architecture.

B. Kernels For Infinite-Width Recurrent Neural Networks

We review the derivation of the CK and NTK of multi-layer (simple) RNN [29] when the inputs are of the same length.

This enables us to investigate practicality of RNN-based kernels by comparing it to standard kernels and NTK on tasks involving non time-series data. This focus on simplified form of kernels leads to a fast GPU implementation of computation on the whole input signal set, which we will discuss in section IV.

Given a data sequence $\mathbf{x} = \{\mathbf{x}_t\}_{t=1}^T$ of fixed length T with data at time step t , $\mathbf{x}_t \in \mathbb{R}^m$, an RNN with n units in each hidden layer performs the following recursive computation at each layer and each time step

$$\begin{aligned} \mathbf{g}^{(1,t)}(\mathbf{x}) &= \frac{\sigma_w}{\sqrt{n}} \mathbf{W}^{(1)} \mathbf{h}^{(1,t-1)}(\mathbf{x}) + \frac{\sigma_u}{\sqrt{m}} \mathbf{U}^{(1)} \mathbf{x}_t + \sigma_b \mathbf{b}^{(1)} \\ \mathbf{g}^{(\ell,t)}(\mathbf{x}) &= \frac{\sigma_w}{\sqrt{n}} \mathbf{W}^{(\ell)} \mathbf{h}^{(\ell,t-1)}(\mathbf{x}) + \frac{\sigma_u}{\sqrt{n}} \mathbf{U}^{(\ell)} \mathbf{h}^{(\ell-1,t)}(\mathbf{x}) + \sigma_b \mathbf{b}^{(\ell)} \\ \mathbf{h}^{(\ell,t)}(\mathbf{x}) &= \phi(\mathbf{g}^{(\ell,t)}(\mathbf{x})) \end{aligned}$$

where $\mathbf{W}^{(\ell)} \in \mathbb{R}^{n \times n}$, $\mathbf{b}^{(\ell)} \in \mathbb{R}^n$ for $\ell \in [L]$ with $[L] = \{1, \dots, L\}$, $\mathbf{U}^{(1)} \in \mathbb{R}^{n \times m}$ and $\mathbf{U}^{(\ell)} \in \mathbb{R}^{n \times n}$ for $\ell \geq 2$, and $\phi(\cdot) : \mathbb{R} \rightarrow \mathbb{R}$ is the activation function that acts entry-wise on a vector. In this paper, we will consider the rectified linear unit (ReLU) $\phi(x) = \max(0, x)$.

By definition, $\mathcal{N}(\boldsymbol{\mu}, \boldsymbol{\Sigma})$ represents the multidimensional Gaussian distribution with mean vector $\boldsymbol{\mu}$ and covariance matrix $\boldsymbol{\Sigma}$. We set the initial hidden state in all layers to zero, i.e, $\mathbf{h}^{(\ell,0)}(\mathbf{x}) = 0$. The (possibly multi dimensional) output of an RNN with L hidden layers is typically a linear transformation of the hidden layer of the last layer L and the time t

$$f_{\theta}^{(t)}(\mathbf{x}) = \frac{\sigma_v}{\sqrt{n}} \mathbf{V}^{(t)} \mathbf{h}^{(L,t)}(\mathbf{x}) \in \mathbb{R}^d.$$

In this section, we are interested in only the output of the last time step, i.e $f_{\theta}^{(T)}(\mathbf{x}) = \frac{\sigma_v}{\sqrt{n}} \mathbf{V}^{(T)} \mathbf{h}^{(L,T)}(\mathbf{x})$. The learnable parameters

$$\theta = \text{vect}[\{\{\mathbf{W}^{(\ell)}, \mathbf{U}^{(\ell)}, \mathbf{b}^{(\ell)}\}_{\ell=1}^L, \mathbf{V}^{(T)}\}], \quad (3)$$

are initialized from a $\mathcal{N}(0, 1)$ random variable and the variance of weights appear as an scaling factor of weights, forming the initialization hyperparameters

$$\sigma = \{\sigma_w, \sigma_u, \sigma_b, \sigma_v\}.$$

Leveraging the equivalence of infinite-width DNNs with Gaussian processes (GPs) [2]–[6], as $n \rightarrow \infty$, each coordinate of the RNN output converges to a GP with the CK

$$\mathcal{K}^{(T)}(\mathbf{x}, \mathbf{x}') = \mathbb{E}_{\theta \sim \mathcal{N}} [[f_{\theta}^{(T)}(\mathbf{x})]_i \cdot [f_{\theta}^{(T)}(\mathbf{x}')]_i], \quad \forall i \in [d].$$

The pre-activation $\mathbf{g}^{(\ell,t)}(\mathbf{x})$ and gradient vectors $\boldsymbol{\delta}^{(\ell,t)}(\mathbf{x}) := \sqrt{n}(\nabla_{\mathbf{g}^{(\ell,t)}(\mathbf{x})} f_{\theta}(\mathbf{x}))$ also converge to zero mean GPs with kernels

$$\Sigma^{(\ell,t)}(\mathbf{x}, \mathbf{x}') = \mathbb{E}_{\theta \sim \mathcal{N}} [[\mathbf{g}^{(\ell,t)}(\mathbf{x})]_i \cdot [\mathbf{g}^{(\ell,t)}(\mathbf{x}')]_i] \quad \forall i \in [n], \quad (4)$$

$$\Pi^{(\ell,t)}(\mathbf{x}, \mathbf{x}') = \mathbb{E}_{\theta \sim \mathcal{N}} [[\boldsymbol{\delta}^{(\ell,t)}(\mathbf{x})]_i \cdot [\boldsymbol{\delta}^{(\ell,t)}(\mathbf{x}')]_i] \quad \forall i \in [n]. \quad (5)$$

The NTK of RNN for two inputs $\mathbf{x} = \{\mathbf{x}_t\}_{t=1}^T$ and $\mathbf{x}' = \{\mathbf{x}'_t\}_{t=1}^T$ can thus be obtained as

$$\begin{aligned} \Theta(\mathbf{x}, \mathbf{x}') &= \langle \nabla_{\theta} f_{\theta}^{(T)}(\mathbf{x}), \nabla_{\theta} f_{\theta}^{(T)}(\mathbf{x}') \rangle = \\ &\left(\sum_{\ell=1}^L \sum_{t=1}^T (\Pi^{(\ell,t)}(\mathbf{x}, \mathbf{x}') \cdot \Sigma^{(\ell,t)}(\mathbf{x}, \mathbf{x}')) + \mathcal{K}^{(T)}(\mathbf{x}, \mathbf{x}') \right) \otimes \mathbf{I}_d, \end{aligned} \quad (6)$$

where \mathbf{I}_d is the identity matrix of size d . For more details on the derivation of CK and NTK of RNN see [20].

III. INFINITE-WIDTH BIDIRECTIONAL AND AVERAGE POOLING RECURRENT NEURAL NETWORKS KERNELS

In this section, we derive the CK and NTK of different variants of RNNs: bidirectional RNN, RNN with average pooling and their combination. Our derivations is built upon the formula for the CK and NTK of the single output in the last time step in equations 4, 5, 6 and the following lemma introduced in [6], [25], [28].

Lemma 1: let $\mathbf{h}(\mathbf{x})$ and $\bar{\mathbf{h}}(\mathbf{x}')$ be two arbitrary hidden states in an infinite width DNN with a set of parameters θ with different possible inputs. We take two outputs of the form $y(\mathbf{x}) = \frac{\sigma_v}{\sqrt{n}} \mathbf{V} \mathbf{h}(\mathbf{x})$ and $\bar{y}(\mathbf{x}') = \frac{\sigma_v}{\sqrt{n}} \bar{\mathbf{V}} \bar{\mathbf{h}}(\mathbf{x}')$, where $\mathbf{V}, \bar{\mathbf{V}} \in \mathbb{R}^{n \times d}$ are drawn *independently*

from Gaussian distribution. As a result, the following quantities, regardless of DNN architecture, are always zero

$$\begin{aligned}\mathbb{E}_{\theta \sim \mathcal{N}} [y_i(\mathbf{x}) \times \bar{y}_j(\mathbf{x}')^T] &= \mathbf{0}_d \\ \langle \nabla_{\theta} y(\mathbf{x}), \nabla_{\theta} \bar{y}(\mathbf{x}') \rangle &= \mathbf{0}_d,\end{aligned}$$

Where $\mathbf{0}_d$ is a $d \times d$ matrix with all zero entries.

A. Recurrent Neural Networks With Average Pooling

In This section we derive the CK and NTK of RNN with average pooling. Average pooling is defined as follows

$$f_{\theta}^{\text{avg}}(\mathbf{x}) = \sum_{t=1}^T \frac{\sigma_v}{\sqrt{n}} \mathbf{V}^{(t)} \mathbf{h}^{(L,t)}(\mathbf{x}) = \sum_{t=1}^T f_{\theta}^{(t)}(\mathbf{x}).$$

Because here we consider data points of the same length, we have a fixed architecture and we use different weights at the output and have a fixed parameter space. As a result, $\theta = \text{vect}[\{\{\mathbf{W}^{(\ell)}, \mathbf{U}^{(\ell)}, \mathbf{b}^{(\ell)}\}_{\ell=1}^L, \{\mathbf{V}^{(t)}\}_{t=1}^T\}]$ forms the fixed parameters set. Hence, the NTK becomes

$$\begin{aligned}\Theta^{\text{avg}}(\mathbf{x}, \mathbf{x}') &= \langle \nabla_{\theta} f_{\theta}^{\text{avg}}(\mathbf{x}), \nabla_{\theta} f_{\theta}^{\text{avg}}(\mathbf{x}') \rangle \\ &= \sum_{t=1}^T \sum_{t'=1}^T \langle \nabla_{\theta} f_{\theta}^{(t)}(\mathbf{x}), \nabla_{\theta} f_{\theta}^{(t')}(\mathbf{x}') \rangle \\ &= \sum_{t=1}^T \langle \nabla_{\theta} f_{\theta}^{(t)}(\mathbf{x}), \nabla_{\theta} f_{\theta}^{(t)}(\mathbf{x}') \rangle \\ &= \sum_{t=1}^T \Theta^{(t)}(\mathbf{x}, \mathbf{x}').\end{aligned}$$

Because of lemma 1 and the independence of the output layer weights of each time we have

$$\langle \nabla_{\theta} f_{\theta}^{(t)}(\mathbf{x}), \nabla_{\theta} f_{\theta}^{(t')}(\mathbf{x}') \rangle = 0 \quad t \neq t' \quad (7)$$

Similarly, for the CK we have

$$\begin{aligned}\mathcal{K}^{\text{avg}}(\mathbf{x}, \mathbf{x}') &= \sum_{t=1}^T \mathbb{E}_{\theta \sim \mathcal{N}} [[f_{\theta}^{(t)}(\mathbf{x})]_i \cdot [f_{\theta}^{(t)}(\mathbf{x}')]_i] \\ &= \sum_{t=1}^T \mathcal{K}^{(t)}(\mathbf{x}, \mathbf{x}').\end{aligned} \quad (8)$$

Each $\Theta^{(t)}(\mathbf{x}, \mathbf{x}')$ and $\mathcal{K}^{(t)}(\mathbf{x}, \mathbf{x}')$ can be thought of as NTK and CK kernels of an RNN with single output at last time step when the first t data points are fed to the network.

Remark. Another way to do average pooling is to use same weights for the output at each time step, i.e.,

$$f_{\theta}^{\text{avg}}(\mathbf{x}) = \sum_{t=1}^T \frac{\sigma_v}{\sqrt{n}} \mathbf{V} \mathbf{h}^{(L,t)}(\mathbf{x}),$$

which is necessary to deal with signals of different lengths. This way the final NTK will contain the information between different time steps, as equation 7 will have a nonzero value. However, calculating the NTK with this pooling strategy requires storing a tensor of dimension $(T \times T \times N \times N)$, where N is the number of data and T the data length. While block computation and approximations could be developed for such cases, we instead concentrate on the pooling strategy discussed above as it provides an out-of-the-box tractable solution. For further details, see [28] on how the NTK of a single layer RNN with average pooling using the same output weight is calculated.

B. Bidirectional Recurrent Neural Networks

In this section, we derive the CK and NTK of bidirectional RNNs. In BI-RNNs, the original signal \mathbf{x} is fed into a simple RNN with parameters θ in equation 3 and hyperparameters σ to calculate hidden states $\mathbf{h}^{(\ell,t)}(\mathbf{x})$ and output $f_{\theta}^{(T)}(\mathbf{x})$. In addition, the flipped version of the signal \mathbf{x} , i.e. $\bar{\mathbf{x}} = \{\mathbf{x}_{T-t}\}_{t=0}^{T-1}$, is fed to another simple RNN structure with the same initialization hyperparameters σ , but parameters $\bar{\theta}$ are an iid copies of θ to produce $\bar{\mathbf{h}}^{(\ell,t)}(\bar{\mathbf{x}})$ and $\bar{f}_{\bar{\theta}}^{(T)}(\bar{\mathbf{x}})$. The output of a BI-RNN is simply the sum of the output of two network

$$f_{\bar{\theta}}^{\text{bi}}(\mathbf{x}) = f_{\theta}^{(T)}(\mathbf{x}) + \bar{f}_{\bar{\theta}}^{(T)}(\bar{\mathbf{x}})$$

and $\bar{\theta} = \theta \cup \bar{\theta}$ is the set of all parameters. The NTK of this network becomes

$$\begin{aligned}\Theta^{\text{avg}}(\mathbf{x}, \mathbf{x}') &= \langle \nabla_{\bar{\theta}} f_{\bar{\theta}}^{\text{bi}}(\mathbf{x}), \nabla_{\bar{\theta}} f_{\bar{\theta}}^{\text{bi}}(\mathbf{x}') \rangle \\ &= \langle \nabla_{\theta} f_{\theta}^{(T)}(\mathbf{x}), \nabla_{\theta} f_{\theta}^{(T)}(\mathbf{x}') \rangle \\ &\quad + \langle \nabla_{\bar{\theta}} f_{\bar{\theta}}^{(T)}(\bar{\mathbf{x}}), \nabla_{\bar{\theta}} f_{\bar{\theta}}^{(T)}(\bar{\mathbf{x}}') \rangle \\ &\quad + \langle \nabla_{\bar{\theta}} f_{\bar{\theta}}^{(T)}(\bar{\mathbf{x}}), \nabla_{\theta} f_{\theta}^{(T)}(\mathbf{x}') \rangle \\ &\quad + \langle \nabla_{\theta} f_{\theta}^{(T)}(\mathbf{x}), \nabla_{\bar{\theta}} f_{\bar{\theta}}^{(T)}(\bar{\mathbf{x}}') \rangle.\end{aligned} \quad (9)$$

Where the third and the fourth term in equation 9 become zero as a result of lemma 1. As a result, we have:

$$\Theta^{\text{bi}}(\mathbf{x}, \mathbf{x}') = \Theta(\mathbf{x}, \mathbf{x}') + \Theta(\bar{\mathbf{x}}, \bar{\mathbf{x}}'). \quad (10)$$

And similarly

$$\mathcal{K}^{\text{bi}}(\mathbf{x}, \mathbf{x}') = \mathcal{K}^{(T)}(\mathbf{x}, \mathbf{x}') + \mathcal{K}^{(T)}(\bar{\mathbf{x}}, \bar{\mathbf{x}}'). \quad (11)$$

C. Bidirectional Recurrent Neural Networks With Average Pooling

In this section, we derive the NTK and CK of bidirectional RNNs with average pooling. Given the CK and NTK of BI-RNN is respectively the sum of CK and NTK of a simple RNN evaluated on the data and its flipped version, it is easy to generalize the results for a BI-RNN-AVG, where the kernels will be the sum of kernels of RNN-AVG evaluated on both version of input data, i.e:

$$\mathcal{K}^{\text{bi-avg}}(\mathbf{x}, \mathbf{x}') = \mathcal{K}^{\text{avg}}(\mathbf{x}, \mathbf{x}') + \mathcal{K}^{\text{avg}}(\bar{\mathbf{x}}, \bar{\mathbf{x}}'), \quad (12)$$

$$\Theta^{\text{bi-avg}}(\mathbf{x}, \mathbf{x}') = \Theta^{\text{avg}}(\mathbf{x}, \mathbf{x}') + \Theta^{\text{avg}}(\bar{\mathbf{x}}, \bar{\mathbf{x}}'). \quad (13)$$

Which will conclude the NTK and CK derivation of all mentioned RNN variants.

IV. FAST GPU-BASED IMPLEMENTATION OF RNN-BASED KERNELS

In this section, we provide the implementation details of calculating the kernels associated with infinite width RNNs (CK and NTK) with the same length that are used to obtain the Gram matrices containing the pairwise CK and NTK of inputs. We also demonstrate the running time of calculating the Gram matrices on the CPU and GPU.

A. Infinite-Width Recurrent Neural Network Kernels Pseudo Code

As discussed, kernels associate with RNN can handle data of various lengths. In the case when two inputs have different lengths, the calculation of NTK and CK of two inputs requires an adaptive implementation with respect to the length of inputs, which impedes an efficient parallelization of the computation of the Gram matrix with currently available toolboxes. However, when all the data have the same length, the pairwise calculation of NTK and CK of two inputs follows the same procedure. In this setting, computations can be done at once for all set of inputs using simple matrix computations.

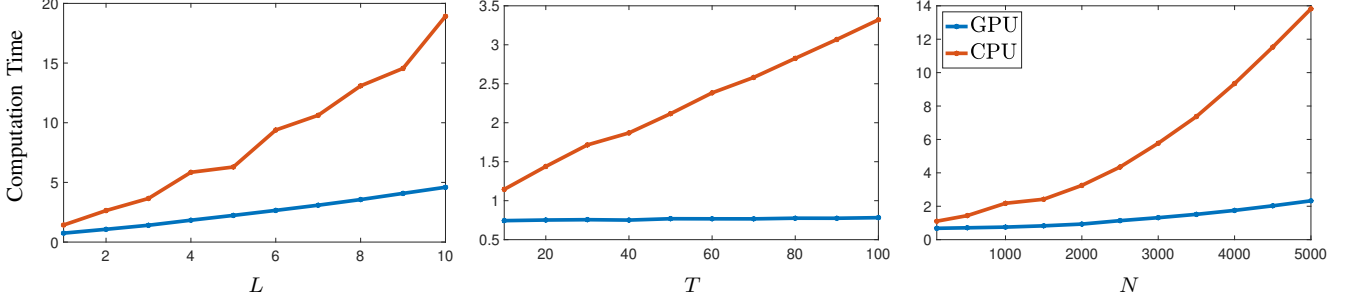


Fig. 2: Visualization of the average computation time over 100 artificial random datasets for GPU (blue) and CPU (red) for different number of RNTK layers (L), data length (T) and number of data points (N). **Left:** $T = 20$, $N = 1000$ and vary L **Middle:** $L = 1$, $N = 1000$ and vary T . **Right:** $L = 1$, $T = 20$ and vary N . Through these three experiments we can see how the GPU implementation significantly reduces the computation time compared to CPU implementation with increasing L , T and N .

Algorithm 1 CK of RNN and RNN-AVG

```

1: for  $t = 1$  do
2:    $\Sigma^{(1,1)}(\mathbf{x}, \mathbf{x}') = \frac{\sigma_d^2}{d} \langle \mathbf{x}_1, \mathbf{x}'_1 \rangle + \sigma_b^2$ 
3:   for  $\ell = 2, \dots, L$  do
4:      $\Sigma^{(\ell,1)}(\mathbf{x}, \mathbf{x}') = \sigma_u^2 V_\phi[\mathbf{K}^{(\ell-1,1)}(\mathbf{x}, \mathbf{x}')] + \sigma_b^2$ 
5:    $\mathcal{K}^{(1)}(\mathbf{x}, \mathbf{x}') = \sigma_v^2 V_\phi[\mathbf{K}^{(L,1)}(\mathbf{x}, \mathbf{x}')] + \sigma_b^2$ 
6:    $\mathcal{K}^{\text{avg}}(\mathbf{x}, \mathbf{x}') = \mathcal{K}^{(1)}(\mathbf{x}, \mathbf{x}')$ 
7: for  $t = 2, \dots, T$  do
8:    $\Sigma^{(1,t)}(\mathbf{x}, \mathbf{x}') = \frac{\sigma_d^2}{d} \langle \mathbf{x}_t, \mathbf{x}'_t \rangle + \sigma_w^2 V_\phi[\mathbf{K}^{(1,t-1)}(\mathbf{x}, \mathbf{x}')] + \sigma_b^2$ 
9:   for  $\ell = 2, \dots, L$  do
10:     $\Sigma^{(\ell,t)}(\mathbf{x}, \mathbf{x}') = \sigma_u^2 V_\phi[\mathbf{K}^{(\ell-1,t)}(\mathbf{x}, \mathbf{x}')] + \sigma_w^2 V_\phi[\mathbf{K}^{(\ell,t-1)}(\mathbf{x}, \mathbf{x}')] + \sigma_b^2$ 
11:    $\mathcal{K}^{(t)}(\mathbf{x}, \mathbf{x}') = \sigma_v^2 V_\phi[\mathbf{K}^{(L,t)}(\mathbf{x}, \mathbf{x}')] + \sigma_b^2$ 
12:    $\mathcal{K}^{\text{avg}}(\mathbf{x}, \mathbf{x}') \leftarrow \mathcal{K}^{\text{avg}}(\mathbf{x}, \mathbf{x}') + \mathcal{K}^{(t)}(\mathbf{x}, \mathbf{x}')$ 
13: CK of RNN:  $\mathcal{K}^{(T)}(\mathbf{x}, \mathbf{x}')$ 
14: CK of RNN-AVG:  $\mathcal{K}^{\text{avg}}(\mathbf{x}, \mathbf{x}')$ 

```

Such computations can be highly parallelized on GPU allowing fast application of kernels associated with infinite width RNNs for kernel-based classification or regression tasks using the SymJAX library [24].

The details of implementations for CK and NTK of RNN and RNN-AVG are provided in algorithms 1 and 2 respectively. The kernels of BI-RNN and BI-RNN-AVG can be easily obtained by summing the outputs the algorithms with the original signal and with the flipped version as inputs as demonstrated in equations 10, 11, 12, and 13.

One key practical advantage of the algorithms 1 and 2 is the memory efficiently. As shown in the general case of different length in [20], the calculation of NTK of RNN requires calculating and storing the GP kernels of pre-activation layers (equation 4) and then gradient layers (equation 5) of *all* time steps and finally use them to calculate the final formula for NTK in equation 2. However, with the assumption of the same length, the calculation of NTK can be done along with the calculation of the GP without directly calculating the GP kernel of gradients in Eq. 5 using the algorithm 2. Such implementation drops the dependency of calculation of NTK from GP kernels of all time steps to GP kernels of the previous and current time step calculated at algorithm 1. As a result, storage space of order $\mathcal{O}(N \times N)$ is needed to calculate the NTK, rather than $\mathcal{O}(T \times N \times N)$, that will be practically crucial for the data of long lengths.

The set of equations in algorithms 1 and 2 depends on an operator $V_\phi[\mathbf{K}]$ that depends on the nonlinearity $\phi(\cdot)$ and a positive semi-

Algorithm 2 NTK of RNN-AVG

```

1: for  $t = 1$  do
2:    $\Psi^{(1,1)}(\mathbf{x}, \mathbf{x}') = \Sigma^{(1,1)}(\mathbf{x}, \mathbf{x}')$ 
3:   for  $\ell = 2, \dots, L$  do
4:      $\Psi^{(\ell,1)}(\mathbf{x}, \mathbf{x}') = \Sigma^{(\ell,1)}(\mathbf{x}, \mathbf{x}') + \sigma_u^2 \Psi^{(\ell-1,1)}(\mathbf{x}, \mathbf{x}') V_{\phi'}[\mathbf{K}^{(\ell-1,1)}(\mathbf{x}, \mathbf{x}')] + \sigma_v^2 \Psi^{(L,1)}(\mathbf{x}, \mathbf{x}') V_{\phi'}[\mathbf{K}^{(L,1)}(\mathbf{x}, \mathbf{x}')] + \sigma_b^2$ 
5:    $\Theta^{(1)}(\mathbf{x}, \mathbf{x}') = \mathcal{K}^{(1)}(\mathbf{x}, \mathbf{x}') + \sigma_v^2 \Psi^{(L,1)}(\mathbf{x}, \mathbf{x}') V_{\phi'}[\mathbf{K}^{(L,1)}(\mathbf{x}, \mathbf{x}')] + \sigma_b^2$ 
6:    $\Theta^{\text{avg}}(\mathbf{x}, \mathbf{x}') = \Theta^{(1)}(\mathbf{x}, \mathbf{x}')$ 
7: for  $t = 2, \dots, T$  do
8:    $\Psi^{(1,t)}(\mathbf{x}, \mathbf{x}') = \Sigma^{(1,t)}(\mathbf{x}, \mathbf{x}') + \sigma_w^2 \Psi^{(1,t-1)}(\mathbf{x}, \mathbf{x}') V_{\phi'}[\mathbf{K}^{(1,t-1)}(\mathbf{x}, \mathbf{x}')] + \sigma_u^2 \Psi^{(\ell-1,t)}(\mathbf{x}, \mathbf{x}') V_{\phi'}[\mathbf{K}^{(\ell-1,t)}(\mathbf{x}, \mathbf{x}')] + \sigma_v^2 \Psi^{(L,t-1)}(\mathbf{x}, \mathbf{x}') V_{\phi'}[\mathbf{K}^{(L,t-1)}(\mathbf{x}, \mathbf{x}')] + \sigma_b^2$ 
9:   for  $\ell = 2, \dots, L$  do
10:     $\Psi^{(\ell,t)}(\mathbf{x}, \mathbf{x}') = \Sigma^{(\ell,t)}(\mathbf{x}, \mathbf{x}') + \sigma_w^2 \Psi^{(\ell,t-1)}(\mathbf{x}, \mathbf{x}') V_{\phi'}[\mathbf{K}^{(\ell,t-1)}(\mathbf{x}, \mathbf{x}')] + \sigma_u^2 \Psi^{(\ell-1,t)}(\mathbf{x}, \mathbf{x}') V_{\phi'}[\mathbf{K}^{(\ell-1,t)}(\mathbf{x}, \mathbf{x}')] + \sigma_v^2 \Psi^{(L,t)}(\mathbf{x}, \mathbf{x}') V_{\phi'}[\mathbf{K}^{(L,t)}(\mathbf{x}, \mathbf{x}')] + \sigma_b^2$ 
11:    $\Theta^{(t)}(\mathbf{x}, \mathbf{x}') = \mathcal{K}^{(t)}(\mathbf{x}, \mathbf{x}') + \sigma_v^2 \Psi^{(L,t)}(\mathbf{x}, \mathbf{x}') V_{\phi'}[\mathbf{K}^{(L,t)}(\mathbf{x}, \mathbf{x}')] + \sigma_b^2$ 
12:    $\Theta^{\text{avg}}(\mathbf{x}, \mathbf{x}') \leftarrow \Theta^{\text{avg}}(\mathbf{x}, \mathbf{x}') + \Theta^{(t)}(\mathbf{x}, \mathbf{x}')$ 
13: NTK of RNN:  $\Theta^{(T)}(\mathbf{x}, \mathbf{x}')$ 
14: NTK of RNN-AVG:  $\Theta^{\text{avg}}(\mathbf{x}, \mathbf{x}')$ 

```

definite matrix $\mathbf{K} \in \mathbb{R}^{2 \times 2}$

$$V_\phi[\mathbf{K}] = \mathbb{E}[\phi(z_1) \cdot \phi(z_2)], \quad (z_1, z_2) \sim \mathcal{N}(0, \mathbf{K}).$$

In case of $\phi = \text{ReLU}$, an analytical formula for $V_\phi[\mathbf{K}]$ and $V_{\phi'}[\mathbf{K}]$ exists [30]. For any positive definite matrix $\mathbf{K} = \begin{bmatrix} K_1 & K_3 \\ K_3 & K_2 \end{bmatrix}$ we have:

$$V_\phi[\mathbf{K}] = \frac{1}{2\pi} \left(c(\pi - \arccos(c)) + \sqrt{1 - c^2} \right) \sqrt{K_1 K_2},$$

$$V_{\phi'}[\mathbf{K}] = \frac{1}{\pi} (\pi - \arccos(c)).$$

Where $c = K_3 / \sqrt{K_1 K_2}$.

For the specific task of RNN kernels computation, the $\mathbf{K}^{(\ell,t)}(\mathbf{x}, \mathbf{x}')$ is defined as:

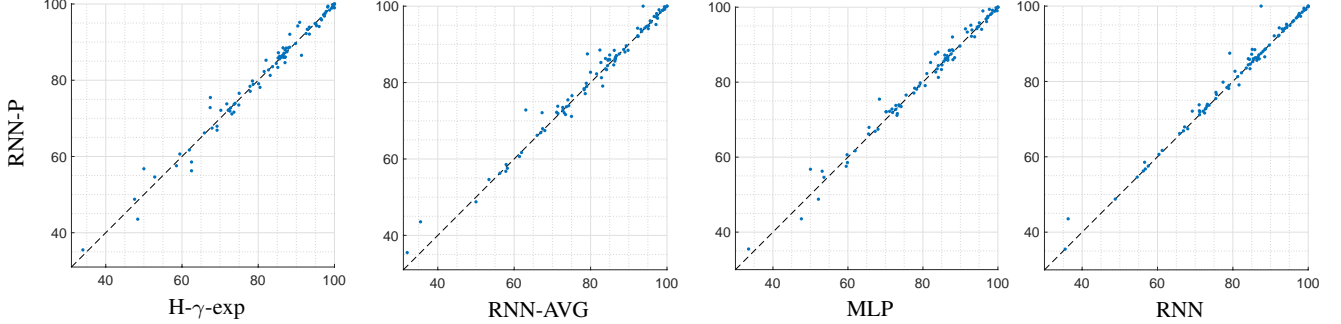
$$\mathbf{K}^{(\ell,t)}(\mathbf{x}, \mathbf{x}') = \begin{bmatrix} \Sigma^{(\ell,t)}(\mathbf{x}, \mathbf{x}) & \Sigma^{(\ell,t)}(\mathbf{x}, \mathbf{x}') \\ \Sigma^{(\ell,t)}(\mathbf{x}, \mathbf{x}') & \Sigma^{(\ell,t)}(\mathbf{x}', \mathbf{x}') \end{bmatrix}.$$

B. CPU And GPU Computation Times

In this section, we present a detailed comparison between CPU and GPU computation of the proposed NTK implementation. More

TABLE I: Summary of non time-series classification results on 90 UCI datasets. RNN-P outperforms all other methods.

	RF	RBF	Polynomial	MLP	H- γ -exp	RNN	BI-RNN	RNN-AVG	BI-RNN-AVG	RNN-P
Acc. mean \uparrow	81.56%	81.03%	80.91%	81.95%	82.25%	81.73%	81.94%	81.75%	82.07%	82.34%
Acc. std	13.90%	15.09%	14.10%	14.10%	14.07%	14.24%	14.47%	14.43%	14.45%	14.06%
P95 \uparrow	81.11%	81.11%	70.00%	84.44%	87.78%	83.33%	84.44%	82.22%	87.78%	86.67%
PMA \uparrow	96.88%	96.09%	96.13%	97.33%	97.71%	97.00%	97.22%	96.97%	97.38%	97.80%
Friedman Rank \downarrow	5.58	5.60	6.27	4.83	4.30	5.16	4.92	5.16	4.28	4.22

Fig. 3: The pairwise comparison of RNN-P with H- γ -exp, RNN-AVG, MLP, and RNN

specifically, we implement NTK as per algorithm 2 and use an artificial dataset in order to control the number of data points, and the dimension and length of the samples to provide CPU and GPU computation benchmarks. For the CPU computation, the used hardware is a 10-core Intel CPU i9-9820X with 62G of RAM. For the GPU configuration, we used a single Nvidia GTX2080Ti card. In both cases the used hardware was installed on a desktop computer. We provide in Figure. 2 the CPU and GPU computation times for varying dataset parameters and observe two key observations. First, the GPU implementation is highly efficient when processing data with increasing length. The number of data points is also efficiently handled and the algorithm sees only an about 2.5X slowdown by using 10 times more samples. The number of layers L seems to be the current bottleneck in the GPU implementation which is due to the intricate inter-layer computation dependencies preventing simple parallelization. In all cases, the GPU implementation sees linear or sub-linear computation time increase when increasing any of those parameters while CPU implementation sees from exponential to linear computation time increases.

We provide all implementations on Github as https://github.com/moonlightlane/RNTK_UCI, implementations are done in SymJAX [24] that benefits from a highly optimized XLA backend compilation providing optimized CPU or GPU executions. We believe that our efficient implementation of NTK and CK of RNNs provides practitioners a novel and powerful kernel for solving practical big data problems.

V. EXPERIMENTS

In this section, we empirically validate the kernels for each RNN variant developed in the previous sections in the context of a C-SVM classifier. The use of SVM classifiers using NTKs, instead of kernel ridge regression, is not equivalent to training of any infinite-width DNN, but yields state-of-the-art (SOTA) performance for classification task as shown in [13]. In this experiments, we use the same datasets used in [13], that includes *non time-serie* 90 UCI pre-processed datasets from UCI data repository [31] with with number of samples less than 5000.

Performances and model comparison. We compare our methods with the top classifiers evaluated in [32], which are Random Forests (RF) (the best performing method based on all the comparison done

in that paper) and polynomial and Gaussian kernel SVM. In addition to those conventional methods, we also compare against the recently derived MLP NTK with C-SVM [13] and against a combination of Laplace and exponential kernels known as H- γ -exp [33] which delivers the best performance on those datasets among the previous mentioned techniques.

Cross-validation and testing procedure. The training procedure follows [13] and [32]. First, each dataset is divided into two subsets of equal size; one is used for training and the other for validation and thus cross-validation. After cross-validation has been completed and the best hyper-parameters (based on the validation set performance) have been obtained, the test accuracy is computed by averaging the accuracy of K -fold cross testing with $K = 4$. That is, the dataset is split into 4 folds, 3 of which are used for training, based on the validation set's best hyperparameter, and the test accuracy is obtained from the remaining fold. This process is repeated for all 4 folds. The average accuracy of those 4 test set is denoted as the overall model test accuracy. Like all other previous works, we use the same splitting indices given by [32].

In general, we note hyperparameters for any of those (recurrent) kernels could be selected based on a priori knowledge about the data and the task at hand based on a *sensitivity* analysis [20]. That is, one can pre-select a set of valid hyper-parameters by studying how do they affect the pairwise input data comparison at each time, $(\mathbf{x}_t, \mathbf{x}'_t)$, and in particular how observations at different times are compared to each other. This is particularly important in applications where one wants to enforce (or discourage) the impact of observation that occurred far in the past, for example, when trying to perform regression for the next time sample. In the present case, as we do not assume any a priori knowledge and want to compare the best possible performance of each model, we employed standard cross-validation. For our model, the hyperparameters that are cross-validated as per the above procedure are the standard deviation of the various RNN parameters (the bias vector, recurrent weight matrix, and input weight matrix) as

$$\begin{aligned}\sigma_u &\in \{0.25, 0.5\} \\ \sigma_b &\in \{0.001, 0.1\} \\ L &\in \{1, 2\}\end{aligned}$$

σ_v merely scales the output of the a selected kernel. In particular,

TABLE II: Number of datasets in which NTK or CK outperforms or ties one another in RNNs with different underlying recurrent architectures and MLP. A two-sided t-test was used to compute the p-values. We see that CK and NTK achieve comparable performance when they are used in an SVM classifier, suggesting that using either of them in practice is reasonable.

	MLP	RNN	BI-RNN	RNN-AVG	BI-RNN-AVG	RNN-P
NTK	30	42	36	35	39	39
CK	27	42	38	38	37	38
Tie	33	12	16	17	14	13
p-value	0.998	0.977	0.909	0.954	0.949	0.888

depending on the type of kernel used (BI-RNN, AVG-RNN and so on) this parameter can be adjusted specifically to allow the final pairwise kernel output to have similar scaling with respect to the C-SVM cost. Therefore, we use $\sigma_v = 1$ for simple RNN, $\sigma_v = \frac{1}{\sqrt{2}}$ for BI-RNN, $\sigma_v = \frac{1}{\sqrt{T}}$ for AVG-RNN with pooling size of T , and $\sigma_v = \frac{1}{\sqrt{2T}}$ for BI-RNN-AVG with a pooling of size T . Based on the sensitivity analysis presented in [20], we set $\sigma_w = \sqrt{2}$ in order for the kernel to consider equally all observations from different time-steps. This results directly from utilizing non time-series data (all dimensions matter equally a priori).

Because we chose C-SVM as our classification method, we have an additional set of hyper-parameters to cross-validate

$$C \in \{0.01, 1, 100, 10000, 1000000\}.$$

Those set of hyper-parameters are cross-validated independently for each dataset.

One remaining hyperparameter to consider is the sequence ordering of the input data. Note that generally RNNs leverage the intrinsic ordering of time-series data in time to perform sequential computation in order to learn the mapping function. However, for non-time-series data, there does not exist a natural ordering of the dimensions and any permutation of dimensions is valid and results in a new kernel. As a result, for data with dimension T , $T!$ permutations exist, and performing standard cross-validation on all of those permutations would become quickly intractable. In this paper, we only consider the *default* dimension ordering and its *flip* (i.e., $[1, 2, 3, 4]$ becomes $[4, 3, 2, 1]$) which is a common practice in the context of RNNs. We denote the configuration of a simple RNN that leverages the permutation of the input data as RNN-P. Notice that such flipping does not affect any of the kernels that are based on the BI-RNN, since by design both versions are only modeled internally. As we will see, considering only those two cases will be enough for RNN-P kernels to reach and surpass other methods.

Lastly, for each set of hyperparameters, we use *both* CK and NTK of the different RNN architectures (simple RNN, BI-RNN, RNN-AVG, BI-RNN-AVG, RNN-P) and pick the kernel with the best performance.

An important experimental detail concerns the case where there would exist multiple hyperparameters producing the best validation performance. In the mentioned scenario, we incorporate all the best hyperparameters as separate models and employ voting (between those models) on the test set. This provides a generic and principled method to deal with the problem of heuristically selecting the model, in which we saw that difference between the worst and best model can result in almost half a percent average accuracy across all data sets.

Results. We report the average test accuracy (Acc mean) and the standard deviation (Acc. std) for all datasets. For a more detailed analysis of the results, we also calculate the PMA which is the percentage of the datasets in which a classifier achieves the maximum accuracy across all models. Additionally, we provide the P95 metric, which is the fraction of datasets in which the classifier achieves at

least 95% of the maximum achievable accuracy for each dataset obtained from all models being compared. Lastly, we also provide the Friedman ranking used in [31], which is simply the average of rankings of classifiers for a dataset, among all datasets. Thus, a better performing model must achieve a higher score in all the metrics except for the Friedman ranking in which case lower is better. Those metrics are reported in Table I for all the models. First, we observe that H- γ -exp and BI-RNN-AVG achieve higher P95 values, demonstrating those two methods' ability to consistently produce near state-of-the-art performances. Yet, when considering all other metrics, we observe that RNN-P achieves better performances. The reduction in P95 for RNN-P can be attributed to the presence of a few datasets in which this method achieves less than 95% of the best method. This might be due to the use of non-time-series data coupled with a recurrent kernel in which case the induced underlying modeling of consecutive time-steps (dimension of the input) might lead to greater bias. Taking everything into account, we see significant performance gains across all other metrics for RNN-P, which should motivate practitioners to consider RNN-P as a novel baseline kernel even for non-time-series data.

To visualize the comparison between RNN-P and the top 4 classifiers in terms of the average test accuracy, we present the pairwise scatter plot of the test accuracy for all datasets in Figure 3.

Performances of CK versus NTK. Extensive empirical observations in [14] indicates that for different architectures, CK often outperforms NTK in kernel ridge regression setting. To complement those observations, we directly compare the performances of CK and NTK in C-SVM setting for different proposed RNN architectures in this paper and MLP. For RNN based kernels, we use the same hyperparameter settings in section V but use only CK or NTK. As for CK or NTK MLP, we use the experimental setup described in [13].

We show the number of datasets CK or NTK outperforms or ties one another in Table II. We can see that there is clear no significant superiority of kernels on each other using a two-sided t-test between CK and NTK. Considering that the mentioned trend is consistent for both recurrent and fully connected structures, we hypothesize that the underlying reason behind the performance gap between CK and NTK that has been reported in [14] can be attributed to the algorithm for learning: kernel ridge regression or C-SVM. Jointly with the findings of [13], where it has been shown that CK and NTK coupled with C-SVM outperforms kernel ridge regression from a practical view in classification tasks, we believe that our findings will better guide practitioners in the choice of the classification method to employ and researchers in the comparison of those variants in a more principled way.

VI. CONCLUSION AND DISCUSSION

In this paper, we extended the NTK for RNNs to other variants of RNNs such as bi-direction and average pooling as well as providing the code to compute those kernels using the SymJAX library [24] that can be executed using the CPU or GPU. We tested the performance

of kernels induced by infinite width recurrent architectures on 90 datasets of non-time-series data with a small sample size. We showed that learning C-SVM with these kernels achieves high performance even on datasets that a natural ordering of the inputs does not exist and offer the best classifier among all other kernels and random forests. Recall that NTK of RNN has also been reported to achieve superb performance on time-series data [20]. We believe that the reported empirical results along with the provided accessible and fast implementation should push practitioners to use kernels induced by recurrent architecture on datasets of any kind.

ACKNOWLEDGMENTS

This work was supported by NSF grants CCF-1911094, IIS-1838177, and IIS-1730574; ONR grants N00014-18-12571 and N00014-17-1-2551; AFOSR grant FA9550-18-1-0478; DARPA grant G001534-7500; and a Vannevar Bush Faculty Fellowship, ONR grant N00014-18-1-2047.

REFERENCES

- [1] R. M. Neal, *Bayesian Learning for Neural Networks*. PhD thesis, University of Toronto, 1995.
- [2] J. Lee, J. Sohl-dickstein, J. Pennington, R. Novak, S. Schoenholz, and Y. Bahri, “Deep neural networks as gaussian processes,” in *International Conference on Learning Representations*, 2018.
- [3] D. Duvenaud, O. Rippel, R. Adams, and Z. Ghahramani, “Avoiding pathologies in very deep networks,” in *Artificial Intelligence and Statistics*, pp. 202–210, 2014.
- [4] R. Novak, L. Xiao, Y. Bahri, J. Lee, G. Yang, D. A. Abolafia, J. Pennington, and J. Sohl-dickstein, “Bayesian deep convolutional networks with many channels are gaussian processes,” in *International Conference on Learning Representations*, 2019.
- [5] A. Garriga-Alonso, C. E. Rasmussen, and L. Aitchison, “Deep convolutional networks as shallow gaussian processes,” in *International Conference on Learning Representations*, 2019.
- [6] G. Yang, “Tensor programs i: Wide feedforward or recurrent neural networks of any architecture are gaussian processes,” *arXiv preprint arXiv:1910.12478*, 2019.
- [7] A. Jacot, F. Gabriel, and C. Hongler, “Neural tangent kernel: Convergence and generalization in neural networks,” in *Advances in neural information processing systems*, pp. 8571–8580, 2018.
- [8] J. Lee, L. Xiao, S. Schoenholz, Y. Bahri, R. Novak, J. Sohl-Dickstein, and J. Pennington, “Wide neural networks of any depth evolve as linear models under gradient descent,” in *Advances in neural information processing systems*, pp. 8572–8583, 2019.
- [9] B. Adlam and J. Pennington, “The neural tangent kernel in high dimensions: Triple descent and a multi-scale theory of generalization,” 2020.
- [10] G. Yang and H. Salman, “A fine-grained spectral perspective on neural networks,” 2019.
- [11] B. Bordelon, A. Canatar, and C. Pehlevan, “Spectrum dependent learning curves in kernel regression and wide neural networks,” *arXiv preprint arXiv:2002.02561*, 2020.
- [12] B. Adlam and J. Pennington, “Understanding double descent requires a fine-grained bias-variance decomposition,” *Advances in Neural Information Processing Systems*, vol. 33, 2020.
- [13] S. Arora, S. S. Du, Z. Li, R. Salakhutdinov, R. Wang, and D. Yu, “Harnessing the power of infinitely wide deep nets on small-data tasks,” in *International Conference on Learning Representations*, 2020.
- [14] J. Lee, S. S. Schoenholz, J. Pennington, B. Adlam, L. Xiao, R. Novak, and J. Sohl-Dickstein, “Finite versus infinite neural networks: an empirical study,” *arXiv preprint arXiv:2007.15801*, 2020.
- [15] S. Arora, S. S. Du, W. Hu, Z. Li, R. R. Salakhutdinov, and R. Wang, “On exact computation with an infinitely wide neural net,” in *Advances in Neural Information Processing Systems*, pp. 8141–8150, 2019.
- [16] Z. Li, R. Wang, D. Yu, S. S. Du, W. Hu, R. Salakhutdinov, and S. Arora, “Enhanced convolutional neural tangent kernels,” *arXiv preprint arXiv:1911.00809*, 2019.
- [17] D. Bahdanau, K. Cho, and Y. Bengio, “Neural machine translation by jointly learning to align and translate,” *ArXiv e-prints*, vol. 1409.0473, Sept. 2014.
- [18] A. Graves, A.-r. Mohamed, and G. Hinton, “Speech recognition with deep recurrent neural networks,” in *Proc. IEEE Int. Conf. Acoust., Speech and Signal Process. (ICASSP)*, pp. 6645–6649, IEEE, 2013.
- [19] R. Socher, A. Perelygin, J. Wu, J. Chuang, C. D. Manning, A. Ng, and C. Potts, “Recursive deep models for semantic compositionality over a sentiment treebank,” in *Proc. Conf. Empirical Methods Natural Language Process. (EMNLP)*, pp. 1631–1642, Oct. 2013.
- [20] S. Alemohammad, Z. Wang, R. Balestrierio, and R. Baraniuk, “The recurrent neural tangent kernel,” *arXiv preprint arXiv:2006.10246*, 2020.
- [21] S. Alemohammad, H. Babaei, R. Balestrierio, M. Y. Cheung, A. I. Humayun, D. LeJeune, N. Liu, L. Luzi, J. Tan, Z. Wang, *et al.*, “Wearing a mask: Compressed representations of variable-length sequences using recurrent neural tangent kernels,” *arXiv preprint arXiv:2010.13975*, 2020.
- [22] G. Yang, “Tensor programs iii: Neural matrix laws,” *arXiv preprint arXiv:2009.10685*, 2020.
- [23] M. Schuster and K. K. Paliwal, “Bidirectional recurrent neural networks,” *IEEE Transactions on Signal Processing*, vol. 45, no. 11, pp. 2673–2681, 1997.
- [24] R. Balestrierio, “Symjax: symbolic cpu/gpu/tpu programming,” 2020.
- [25] G. Yang, “Scaling limits of wide neural networks with weight sharing: Gaussian process behavior, gradient independence, and neural tangent kernel derivation,” *arXiv preprint arXiv:1902.04760*, 2019.
- [26] K. Huang, Y. Wang, M. Tao, and T. Zhao, “Why do deep residual networks generalize better than deep feedforward networks?—a neural tangent kernel perspective,” *arXiv preprint arXiv:2002.06262*, 2020.
- [27] S. S. Du, K. Hou, R. R. Salakhutdinov, B. Poczos, R. Wang, and K. Xu, “Graph neural tangent kernel: Fusing graph neural networks with graph kernels,” in *Advances in Neural Information Processing Systems*, pp. 5724–5734, 2019.
- [28] G. Yang, “Tensor programs ii: Neural tangent kernel for any architecture,” *arXiv preprint arXiv:2006.14548*, 2020.
- [29] J. L. Elman, “Finding structure in time,” *Cognitive science*, vol. 14, no. 2, pp. 179–211, 1990.
- [30] Y. Cho and L. K. Saul, “Kernel methods for deep learning,” in *Advances in Neural Information Processing Systems*, pp. 342–350, 2009.
- [31] M. Fernández-Delgado, M. Sirsat, E. Cernadas, S. Alawadi, S. Barro, and M. Febrero-Bande, “An extensive experimental survey of regression methods,” *Neural Networks*, vol. 111, pp. 11 – 34, 2019.
- [32] M. Fernández-Delgado, E. Cernadas, S. Barro, and D. Amorim, “Do we need hundreds of classifiers to solve real world classification problems?,” *Journal of Machine Learning Research*, vol. 15, no. 90, pp. 3133–3181, 2014.
- [33] A. Geifman, A. Yadav, Y. Kasten, M. Galun, D. Jacobs, and R. Basri, “On the similarity between the laplace and neural tangent kernels,” *arXiv preprint arXiv:2007.01580*, 2020.